TIRE TECHNICAL REPORT STANDARD PAGE

1. Title and Subtitle
Smart Nanogrids for Safer Roads

2. Author(s)
Farzad Ferdowsi, Ph.D.; Mohammad J Khattak, Ph.D.; Kouhyar Sheida; Mohammad Seyedi; Muhammad A Afridi; Vijaya Gopu, Ph.D., P.E.

3. Performing Organization Name and Address
University of Louisiana-Lafayette
Electrical Engineering / Civil Engineering
131 Rex St
Lafayette, LA, 70503

4. Sponsoring Agency Name and Address
Louisiana Department of Transportation and Development
P.O. Box 94245
Baton Rouge, LA 70804-9245

5. Report No.
FHWA/LA.24/24-5TIRE

6. Report Date
August 2024

7. Performing Organization Code
LTRC Project Number: 24-5TIRE
SIO Number: 1000500

8. Type of Report and Period Covered
Final Report
August 2024

9. No. of Pages
44

10. Supplementary Notes
Conducted in Cooperation with the U.S. Department of Transportation, Federal Highway Administration

11. Distribution Statement
Unrestricted. This document is available through the National Technical Information Service, Springfield, VA 21161.

12. Key Words
Hybrid DC Microgrid; Piezoelectric; Voltage Control; Reinforcement Learning

13. Abstract
This study introduced a resilient control scheme for a hybrid DC microgrid (HDCMG) that integrates solar photovoltaic (PV), battery storage (BESS), and piezoelectric (PE) energy harvesting modules. The microgrid serves as an energy hub for lighting systems in transportation and infrastructure. PE is modeled using real data from a traffic simulator to enhance practicality. The proposed Reinforcement Learning (RL)-based method was tested against four severe failure scenarios: load-side short circuit, sudden load changes, open circuit, and converter failure. The RL-based controller's performance was compared to a Conventional PI controller, showing marginal improvement in one scenario and significant improvement in three others. This indicates that the proposed scheme is a robust option for microgrids with high uncertainty, such as those using solar and PE harvesters for road lighting.

Project Review Committee

Each research project will have an advisory committee appointed by the LTRC Director. The Project Review Committee is responsible for assisting the LTRC Administrator or Manager in the development of acceptable research problem statements, requests for proposals, review of research proposals, oversight of approved research projects, and implementation of findings.

LTRC appreciates the dedication of the following Project Review Committee Members in guiding this research study to fruition.

LTRC Administrator/Manager

Vijaya Gopu, Ph.D., P.E.

Directorate Implementation Sponsor

Chad Winchester, P.E.

DOTD Chief Engineer

Smart Nanogrids for Safer Roads

By
Farzad Ferdowsi, Ph.D.
Mohammad J Khattak, Ph.D.

University of Louisiana-Lafayette
College of Engineering
131 Rex St.
Lafayette, LA, 70503

LTRC Project No. 24-5TIRE
SIO No. 1000500

conducted for
Louisiana Department of Transportation and Development
Louisiana Transportation Research Center

August 2024

Abstract

This study presents a resilient control scheme for a hybrid DC microgrid (HDCMG) integrating solar photovoltaic (PV), battery storage (BESS), and piezoelectric (PE) energy harvesting modules. The microgrid is designed to power lighting systems in transportation and infrastructure, with PE modeled using real traffic data for practicality. The proposed Reinforcement Learning (RL)-based method was tested against four severe failure scenarios: load-side short circuit, sudden load changes, open circuit, and converter failure. Compared to a Conventional PI controller, the RL-based controller showed marginal improvement in one scenario and significant improvement in three others, demonstrating its robustness for microgrids with high uncertainty, such as those using solar and PE harvesters for road lighting systems.

The study highlights the growing importance of renewable energies (REs) in microgrid systems for environmental benefits. While traditional power sources remain dominant, renewable sources such as wind and PV are gaining prominence. Piezoelectric devices, converting environmental vibrations into electrical energy, are explored as supplementary energy sources, particularly for generating electricity in railroads and roadways.

A Material Testing System (MTS) was used to simulate pressure on PE components, improving control and stabilizing voltage fluctuations. The hybrid microgrid includes PV systems, BESS, and PE modules, with detailed explanations of power ratings and converter configurations. The study emphasizes a direct power management strategy, combining low-power PV panels with PE modules, thus providing a cohesive energy solution without batteries. Further research is suggested to assess the economics, reliability, and durability of piezoelectric modules, highlighting the potential of the proposed control scheme to enhance microgrid resilience and efficiency.

Acknowledgments

This work was supported by the Louisiana Transportation Research Center (LTRC).

Table of Contents

List of Tables

List of Figures

Introduction

The integration of renewable energy sources into transportation infrastructure is becoming increasingly important to address environmental concerns and improve energy sustainability. Solar PV systems and piezoelectric devices are particularly promising due to their ability to harness renewable energy. Solar panels convert sunlight into electricity, while piezoelectric modules generate energy from mechanical stress, such as vibrations from passing vehicles. This dual approach not only reduces reliance on conventional energy sources but also enhances the resilience of energy supply systems for critical infrastructure like road lighting.

The primary objective of this research was to develop a robust control strategy for the HDCMG that could efficiently manage the energy flow from these sustainable sources to the road lighting systems. The project aimed to ensure consistent lighting performance, thereby improving road safety, even under varying environmental conditions and load demands. To achieve these objectives, the research team designed a control system that optimizes the energy distribution from the solar PV and piezoelectric modules to the road lights. The system was tested under different scenarios to evaluate its performance and adaptability. The use of advanced control algorithms allowed for real-time adjustments to energy distribution, ensuring that the road lights remained operational and efficient. By leveraging sustainable energy sources, this project not only contributes to reducing the carbon footprint of transportation infrastructure but also enhances public safety through improved road lighting. The successful implementation of this microgrid system demonstrates the potential for renewable energy technologies to play a critical role in modern infrastructure projects.

Literature Review

Renewable energies (REs) have been increasingly popular for modern microgrid (MG) systems because of their environmental safety and ability to address pollution concerns [1]. Although nuclear, hydro, and thermal power generation continue to be the primary sources of power globally [2], wind turbines and photovoltaic (PV) power generation technologies are gradually gaining prominence. However, their effectiveness is heavily reliant on meteorological conditions [3]. As a result, the majority of turbine plants are strategically situated on mountains and seashores to efficiently harness the wind. Alternatively, photovoltaic (PV) systems can be put into buildings and diverse structures, including rooftops and road tactile pavement [2,3]. Another source is piezoelectric (PE) devices, which could convert environmental vibrations into electrical energy. However, their power generation capabilities were not adequate for use as primary sources of power. Instead, they were commonly employed in low-power applications such as sensors, quartz watches, and portable charging devices [4]. The writers in [5] used a buck-boost converter in the absence of sensors to optimize power for PE energy harvesting. Utilizing PE technology for energy harvesting has various benefits. It offers a potential source of sustainability and RE by enabling the conversion of mechanical energy that would otherwise be wasted into electrical power [6]. Nevertheless, due to their affordable price and less demand for maintenance, PE devices are presently being investigated for their possible usage in generating substantial electricity in railroads and roadways [7]. Based on research and road testing conducted by the California Energy Commission, it has been determined that a PE power generation system installed in a single lane of a one-mile road may produce an annual electricity output of 72,800 kilowatt-hours [8]. To provide a workable harvested energy configuration for pedestrian deployment, the study in [9] highlighted the various strain elements that are impacted by the energy produced by a PZT (Lead Zirconate Titanate) energy-harvesting floor tile (EHFT). A variety of methods for obtaining energy from PE sensors are shown in Figure 1, ranging from low-power wearables to energy sources found in pedestrian traffic.

Figure 1. Different Approaches to Piezoelectric Energy Harvesting

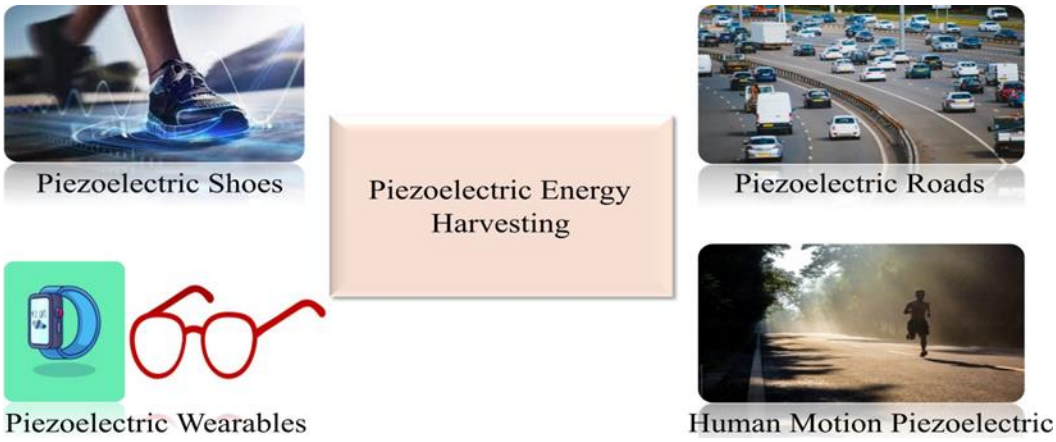

A voltage feedback-based technique was utilized by a power management integrated circuit to harvest energy from PE components [10] and in [11], a PE micro-actuating system was subjected to an adaptive controller, which incorporated an anti-windup compensator. In DC-DC converters, PEs were also employed as resonators. In [12], they were utilized in an inductor-less step-up converter for more efficient operations, and in a self-bias flip rectifier for tracking the maximum power point [13]. Earlier research concentrated on sources and converters separately to increase energy extraction from PE sources or decrease converter size. Yet each source requires its controller when paired with its specific converter. Conversely, [14] introduced a novel approach for hybrid power systems. By using a direct power management strategy to combine a low-power PV panel with a PE harvesting module, this method provides a more cohesive and efficient energy harvesting solution. There is no need for batteries because the system is directly connected to the grid. The study's authors demonstrate the efficiency with which the PE module generates RE. The proposed system lacks an energy storage system (ESS), which may enhance the utilization of the produced RE. It is well known that mechanical vibrations and the surrounding environment have a significant influence on how much energy PV and PE devices can produce. The research team in this study describes a hybrid microgrid (HMG) system in this study that operates in parallel and is intended for smart road applications. The technology combines battery storage (BESS), integrated PE components, and solar PV cells. To create the required voltage, the team used a Material Testing System (MTS) to simulate different pressure situations on the PE components.

The goal in creating a model predictive RL controller for the PE system was to improve control and stabilize abrupt voltage fluctuations. This all-encompassing strategy enhances energy harvesting while guaranteeing steady and dependable power transmission, increasing the usefulness and efficiency of smart infrastructure.

The arrangement of the document is as follows: The experimental results from the MTS machine are presented in Section 2, with a focus on an analysis of the embedded PE sensor performance, which is intended to mimic the impacts of vehicle traffic on a roadway. The MG configuration and the power electronics circuits designed for each energy source are covered in Section 3. In Section 4, the performance of the MG during islanded operation is assessed and the proposed controller is implemented in detail. To evaluate the proposed controller's resilience, Section 5 compares its effectiveness with a conventional Proportional-Integral (PI) controller across a range of fault scenarios. Section 6 outlines the completion of the investigation and provides recommendations for more research.

Objective

The project's primary objective was to improve roadway lighting schemes by incorporating sustainable resources and intelligent control systems. Plans and activities are designed to meet two primary objectives:

- Improve energy diversification that enables enhanced road lighting
- Intelligently control electric power delivery to lights.

Scope

Material Testing Machine and Piezoelectric Data

Testing System

The testing apparatus used for the sample evaluations is the 810 Material Testing System depicted in Figure 3, equipped with servo-hydraulic loop functionalities. During testing, samples were loaded for 0.1 seconds and unloaded for 0.9 seconds, simulating a truck traveling at speeds of 60-70 mph. Two boundary conditions were employed: 1) simply supported and 2) fully supported. Two types of tests were conducted: 1) single haversine waveform loading and 2) multiple haversine waveform loading. Single haversine loading represents a single truck or car moving over the pavement system, while multiple haversine loading simulates two or more trucks with varying loads moving over the pavement system.

Embedment of Piezoelectric Sensors in Fiber-Reinforced Concrete Samples

The PE sensors were embedded at a depth of 1/8 inch from the bottom center of the fiber-reinforced concrete samples. This placement ensures that maximum bending occurs at the center of the sample under load, generating the highest possible voltage due to tensioning. In these samples, the boundary condition was simply supported. The loading frequencies for both single and multiple haversine loading were set at 1 and 10 Hz, with loads ranging from 650 lbf to 3200 lbf. Given that the flexural strength of the fiber-reinforced concrete beam is approximately 5900 lbf, the maximum load was capped at 3200 lbf. The sample of the made concrete is shown in Figure 3. The effects of single and multiple vehicle loads on piezoelectric sensors installed in fiber-reinforced concrete are depicted in Figure 2. The sensors produce a peak voltage of approximately 0.5 V when subjected to a single haversine load; however, when subjected to multiple loads, the voltage decreases to approximately 0.14 V because the concrete’s increased stiffness limits voltage generation and deformation.

Figure 2. Load and voltage profiles for the concrete sample

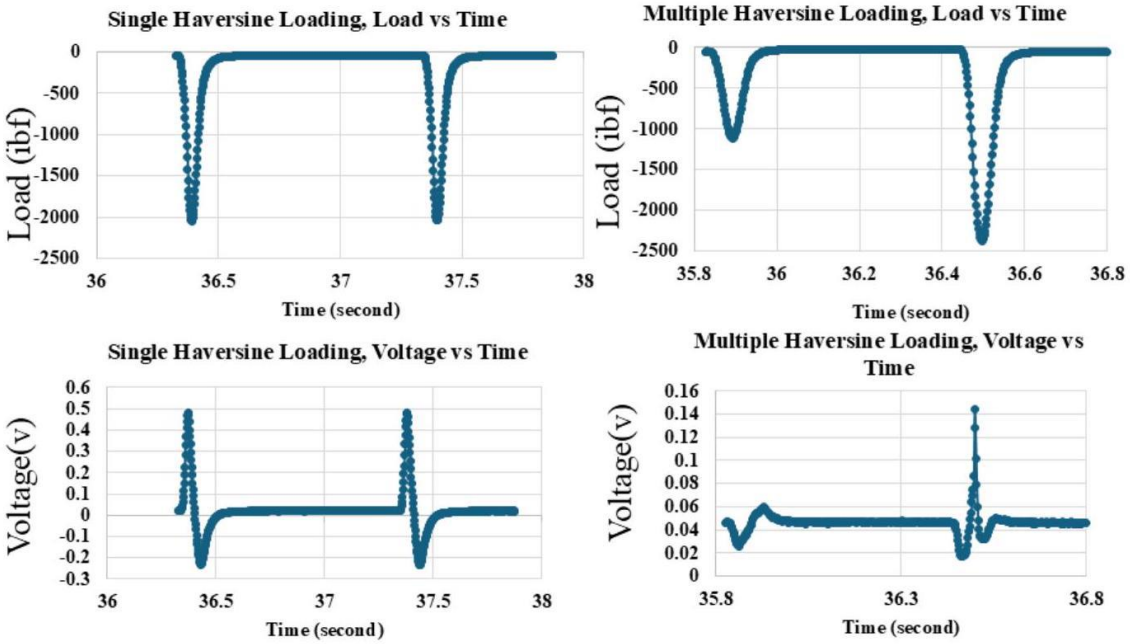

Piezoelectric Sensors in Asphalt Samples

In the asphalt samples, PE sensors were placed between the asphalt and rubber layers to maximize bending and voltage generation when the load was applied. For single haversine loading and multiple haversine loading of asphalt, the loading frequencies were 5 and 10 Hz, with loads ranging from 270 lbf to 370 lbf. In multiple haversine tests, the loading varied from 320 lbf to 400 lbf with frequencies of 1 Hz, 5 Hz, and 10 Hz. For both testing scenarios, the boundary condition was simply supported. The maximum load was set at 400 lbf to avoid exceeding the asphalt's flexural strength of approximately 600 lbf. Figure 5 displays a sample of the manufactured asphalt. The implications of single and multiple vehicle loads on piezoelectric sensors embedded in asphalt are depicted in Figure 4. Since the asphalt is less firm and can withstand more deformation, the sensors can produce up to 10 V when subjected to successive haversine stresses. The material's impact on voltage generation is demonstrated by the fact that, under a single haversine load, the voltage output is likewise larger than in concrete samples for the same reason.

Figure 3. 810 Material Testing System with Concrete Sample

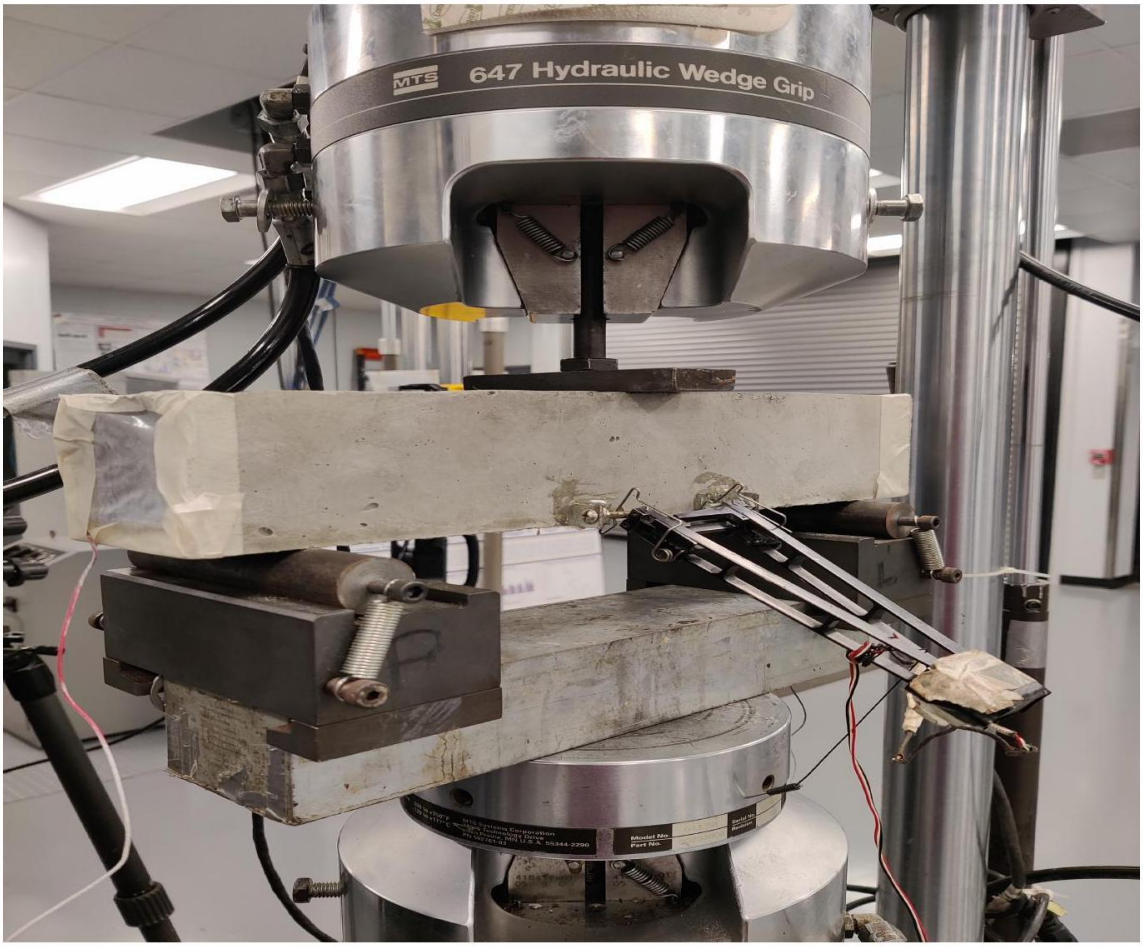

In the fiber-reinforced concrete samples, lower voltage outputs were observed due to their higher stiffness. Conversely, asphalt samples exhibited higher voltage outputs because of their lower stiffness.

Hybrid DC Microgrid Configurations and Setup

In the proposed hybrid power system shown in Figure 6, a PV system, Bess, and PE module are used as power sources. This section offers a comprehensive explanation of each power source, including their power ratings, converter configurations, and detailed mathematical models.

Piezoelectric

The two testing techniques were single-haversine waveform loading and multiple-haversine waveform loading. Single-haversine loading replicates the system of a single truck or car moving on the pavement with a constant load. The movement of two or more trucks over the pavement system while towing varying loads is replicated in multiple haversine testing. In this experiment, the PE model of the Piezo Ceramic Generator SM411 was used. It measures 79x18x1.5 mm and has a static capacitance of 110nF ± 30%. This PE module is displayed in Figure 7. PEs are low-voltage components; thus, to create the necessary voltage for them to be used as a power source on a highway, they must be connected in series.

Figure 4. Load and voltage profiles for the asphalt sample

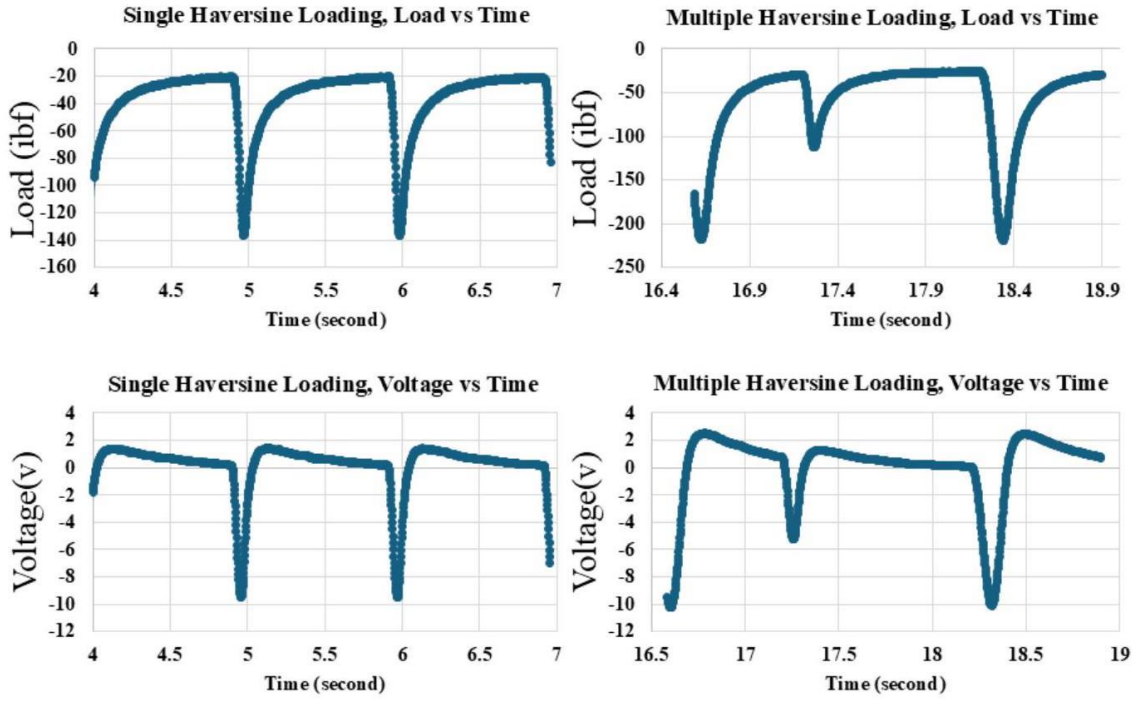

Rectifier

A two-phase harvesting circuit is utilized to optimize power extraction from various dynamic sources. Figure 8 shows this procedure in action. The current produced by the PE components is first transformed into direct current. It is briefly held in a capacitor Ci

while Vin is maintained at the ideal rectifier voltage Vrec. Capacitor (Ci) rectified power is sent to the load bus via a DC-DC converter. Using this technique, the load bus is guaranteed to receive the most power possible from the vibrating PE element. PE modules are connected in series to guarantee the correct output voltage for the controller and boost converter to convert the source bus voltage to the intended load bus voltage.

DC-DC Boost Converter

The boost converter utilizes a high-frequency power switch that alternately charges and discharges the capacitor (C) and inductor (L) via two power electronic switches: a regulated switch (Q) and a diode (D). The general circuit of a boost converter is shown in Figure 10. This model ignores the resistance on the equivalent series resistance of the capacitor, the resistance while the switch is on, and the resistance when the diode is off. The output voltage of the converter can be changed by altering the length of the input pulses; using PWM pulse frequency necessitates a smaller inductor. Equation 1 can be used to determine the duty cycles required for a boost converter in Continuous Conduction Mode in which η is the efficiency of the power conversion.

$$D_{\max} = 1 - \frac{V_{\text{in min}} \times \eta}{V_{\text{Loadbus}}} \tag{1}$$

Figure 5. Asphalt Sample

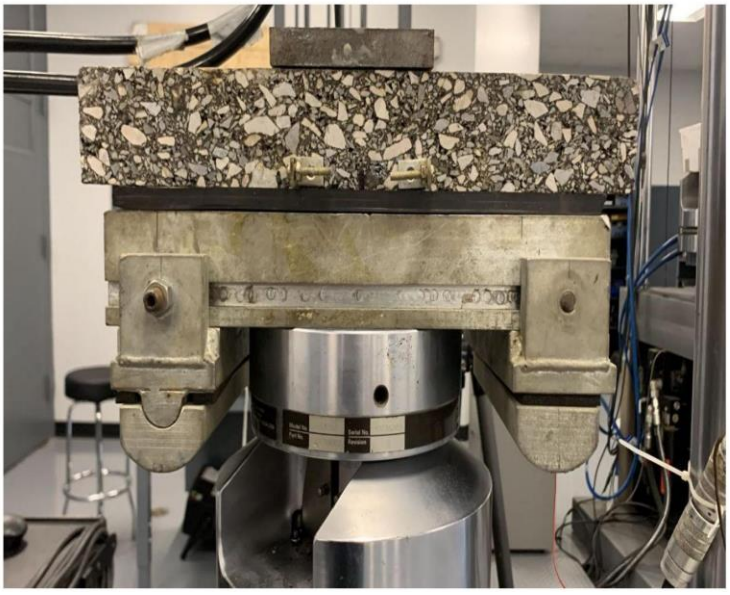

When compared to Continuous Conduction Mode (CCM), the boost converter's operation in Discontinuous Conduction Mode (DCM) is much different. With DCM, every switching cycle results in a zero inductor current. The duty cycle computation is impacted by this. The duty cycle DCM for a boost converter in DCM may be calculated by taking into account the inductor current ripple as well as the energy balance on the inductor and the capacitor. The maximum duty cycle in DCM can be approximated by Equation 2:

$$D_{\mathrm{DCM}} = \frac{1}{1 + \sqrt{\frac{2L \cdot f_s \cdot \eta \cdot V_{\text{Load bus}}}{R \cdot V_{\text{in min}}^2}}} \tag{2}$$

A boost converter exhibits a non-linear relationship between the duty cycle and the output voltage due to the non-linear characteristics of the inductor. The current flow through an inductor increases exponentially as the voltage drop across it decreases exponentially. There is an exponential relationship between the inductors' current and voltage during the charging period. The inductor voltage vl and inductor current i_l have an exponential relationship with the inductor charging time. The voltage across an inductor of a boost converter determines the output voltage in a direct proportion. At a fixed operating frequency, there is a link between the output voltage and duty cycle. This exponential relationship causes a boost converter's output voltage and PWM duty cycle to be non-linear. When the duty cycle increases in a boost converter, the output voltage first climbs until it peaks at a specific point and then starts to fall. Changes in the duty cycle relative to the voltage curve are caused by the load that is connected to the converter. This behavior is depicted in Figure 9.

Solar

Power electronics interfaces, such as DC converters, are necessary to control the DC output voltage produced by a PV system. The DC output voltages generated by PV arrays can be greatly impacted by several parameters, such as irradiance, shadowing effects, ambient temperature, surface cleanliness, and mismatched photovoltaic modules. Solar PV modules are usually coupled in series to boost the voltage output.

Figure 6. Overall Schematic of the Hybrid DC Microgrid

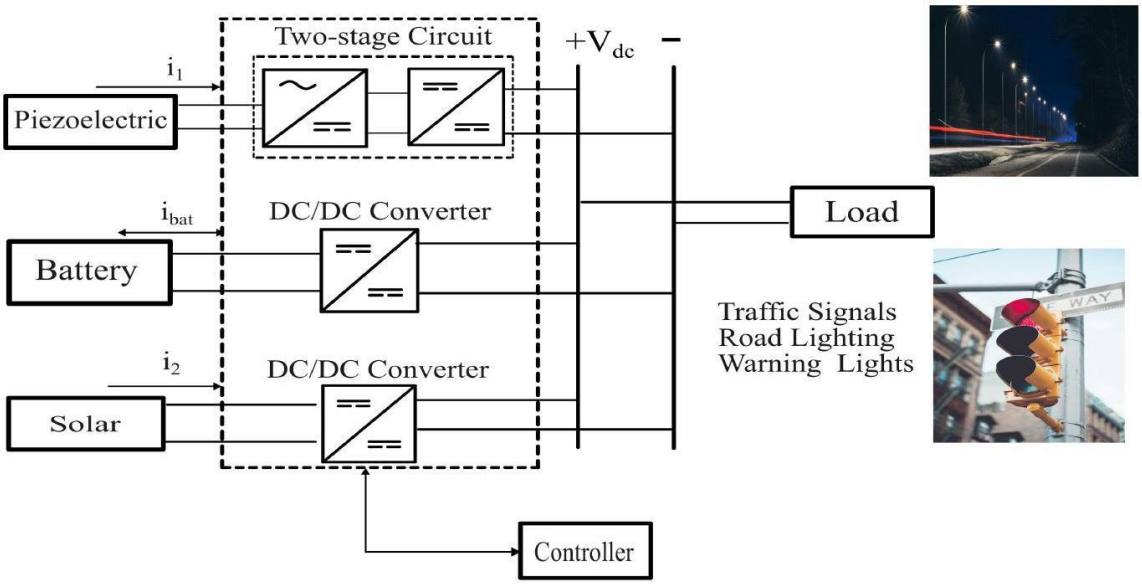

Figure 7. Piezoelectric Sensor

Figure 12 illustrates a basic DC-DC buck converter configuration consisting of a power switch (Q), switching controller, diode (D), inductor (L), capacitor (C), and DC load bus. As a step-down mechanism, the DC-DC buck converter lowers an input voltage to an output value that is consistently less than the input voltage. This simulation, which takes place over a brief time, has 48 volts as the input voltage and 1000 irradiance. With the controller's help, the buck converter lowers the voltage to the load bus voltage. The duty cycle and output voltage of the buck converter have a more linear connection than that of the boost converter. The output voltage increases linearly with an increase in the duty cycle. This happens because the inductor receives the input voltage when the switch is on, and it transfers its energy to the load bus when the switch is off, smoothing the output voltage. Non-idealities including switching losses, parasitic capacitance, and inductor resistance can cause non-linearity in real-world applications. The efficiency and performance of a buck converter are influenced by the internal resistance of the inductor, also known as the series resistance (RL). Figure 11 illustrates this phenomenon.

Battery

The ability of the bidirectional DC converter to switch the direction of power flow and transfer power between two DC sources is well known. To efficiently handle this power transfer—which is essential for battery charging and discharging—two switches work together. Two MOSFETs are used as the switches in this instance. The connection between the load bus and the converter and battery is depicted in Figure 13.

Figure 8. Two-stage Circuit for Piezoelectric Energy Harvesting

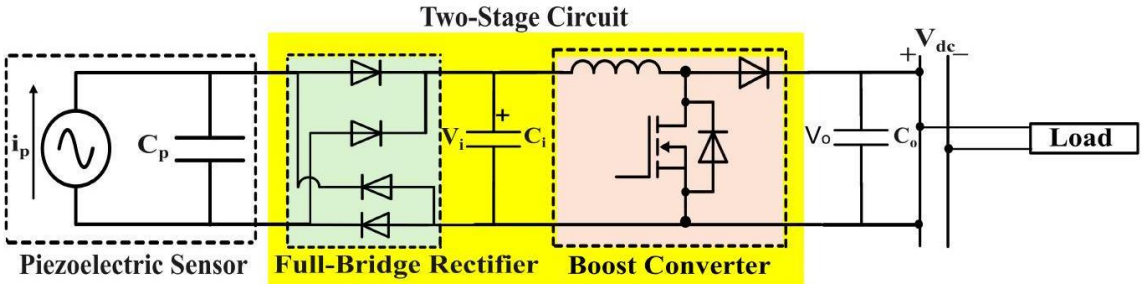

Figure 9. Output Voltage vs Duty cycle with Various Amount of Load for Boost Converter

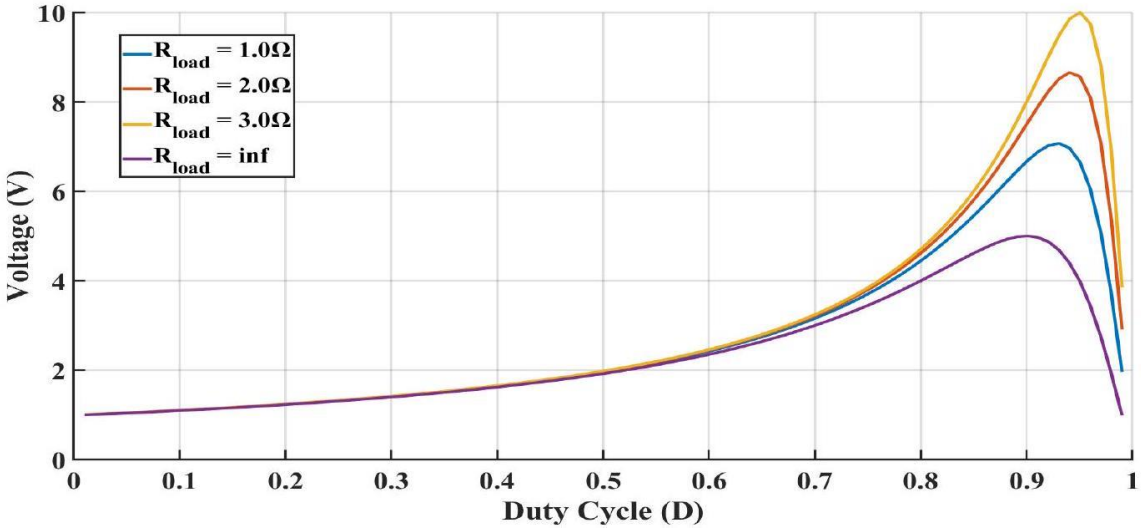

Two finely regulated switches are managed to accomplish the bidirectional conversion. A DC-DC converter that can step up or decrease the input voltage is called a buck-boost converter. It combines the features of boost and buck converters so that, depending on the switch's duty cycle, the output voltage can be either greater or lower than the input voltage. The output voltage Vout in an ideal buck-boost converter is connected to the duty cycle D and input voltage Vin using the following equation:

$$V_{\text{out}} = \frac{D}{1 - D} \times V_{\text{in}} \tag{3}$$

Figure 10. Boost Converter Circuit

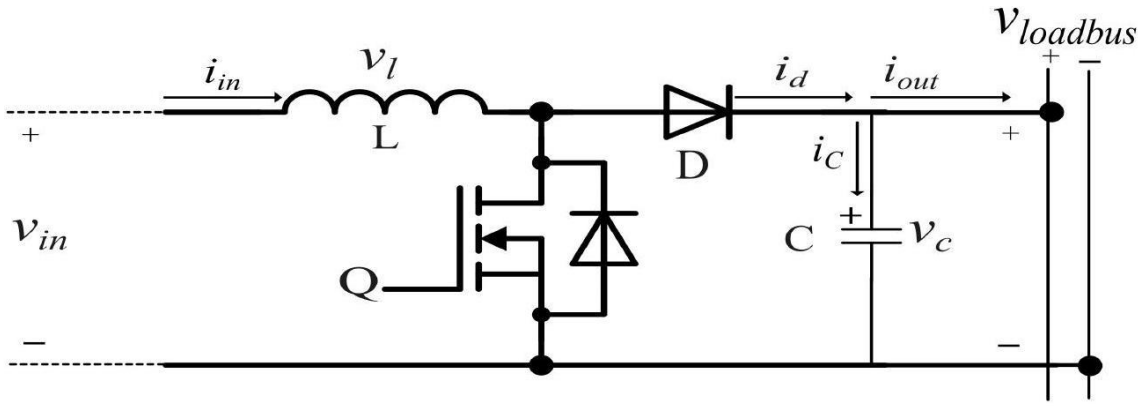

Figure 11. Output Voltage vs Duty cycle with Various Amount of Load for Buck Converter

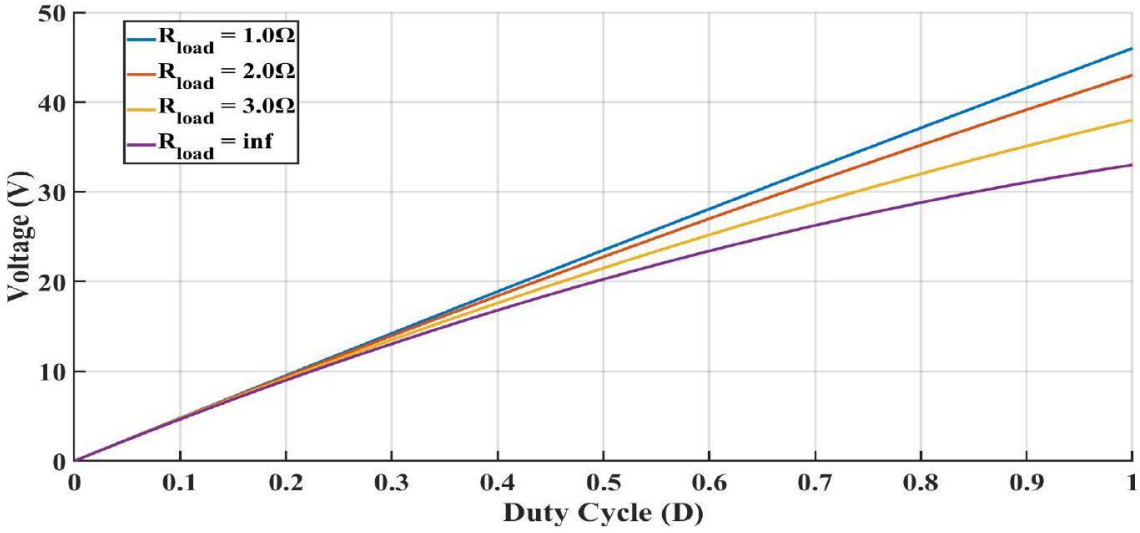

Figure 12. Schematic of a Buck Converter

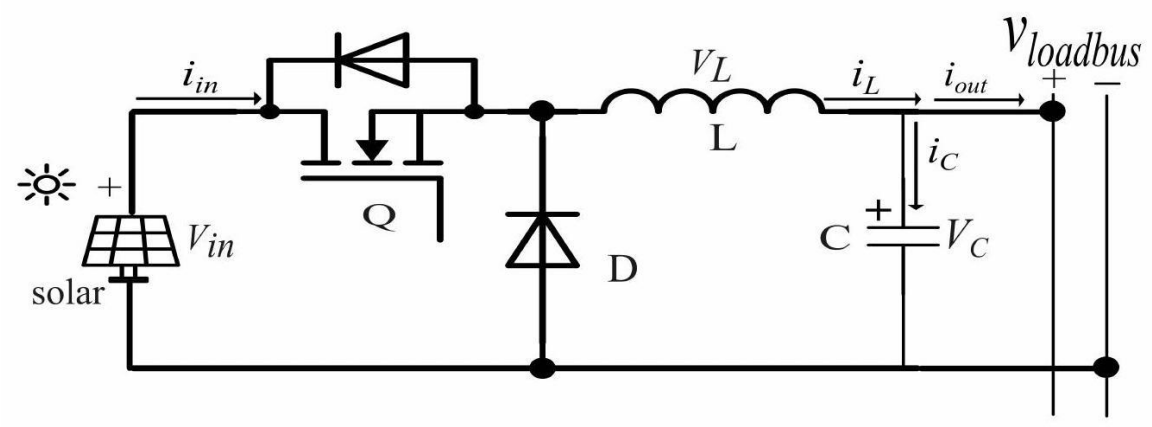

Figure 14 illustrates how this equation shows that for 0 < D < 1, the output voltage grows as the duty cycle increases. A buck-boost converter's performance in real-world applications can be impacted by non-idealities such as switching losses and inductor resistance (RL). Both the buck-boost converter's output voltage and efficiency are impacted by the inductor's internal resistance (RL). The ideal voltage conversion ratio is changed by the voltage drop across RL throughout the on-time and off-time. Approximating the real output voltage Vout in light of the voltage drop across RL is possible.

$$V_{\text{out}} \approx \frac{D \times (V_{\text{in}} - i_l \times R_L)}{1 - D} \tag{4}$$

Where the average inductor current is denoted by i_l.

This formula demonstrates how the output voltage is decreased by the RL. Because of the unique design of the converter, the output voltage in a buck-boost is negative. A negative output voltage is produced when the input voltage's polarity is reversed by the buck-boost converter [15]. The configuration of the switching elements and inductor causes this inversion. Furthermore, the buck-boost converter in our system functions as a boost converter because the battery is in discharge mode. The configuration of the proposed DCHMG can be seen in TABLE 1.

Figure 13. Schematic of a Buck-Boost Converter with Battery Source

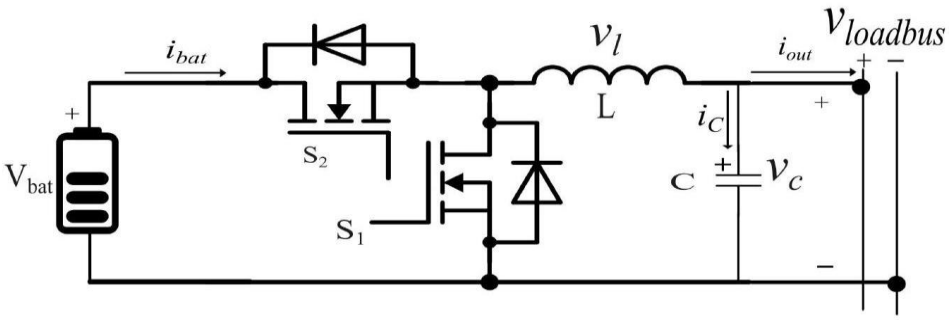

Figure 14. Output Voltage vs Duty cycle with Various Amount of Load for Buck-Boost Converter

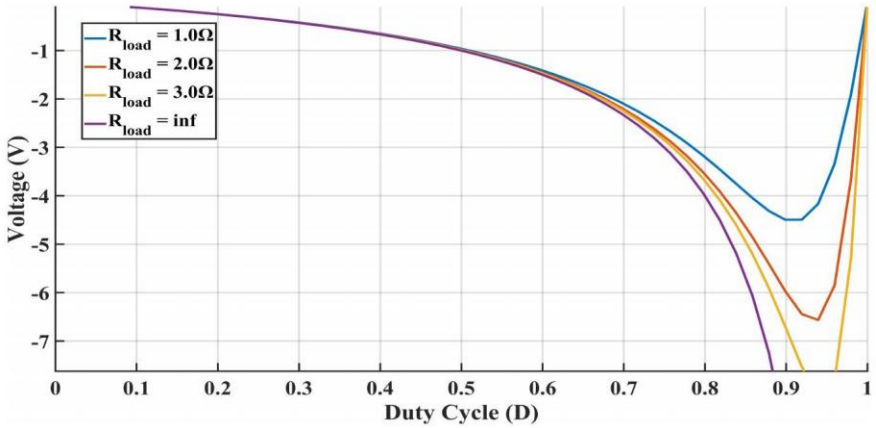

Table 1. Specification of the Hybrid Microgrid

Sources	Specifications	Value
PV	Voltage Open Circuit	48V
	Current Short Circuit	3A
	Irradiance	1000 W/m^2
	Temperature	25 °C
Battery	Nominal Voltage	12V
	Current	3A
	SOC	90%
Piezo	Voltage Range	0~13.5 V
	Max Current/Module	0.8 A

Methodology

Reinforcement Learning

Power electronics and power systems have made substantial use of RL. RL is used in electric cars (EVs) to improve battery utilization and energy management [16]. RL increases efficiency in the field of electrical machines and converters [17], and it enhances autonomy and resilience in MGs [18]. Sequential decision-making under uncertainty can be modeled using the Markov Decision Process (MDP) technique. Various statuses and behaviors are taken into consideration when creating an MDP. It is described as a five-element tuple $(\delta, A, T, R, \gamma)$, in which the action space is represented by $a_t \in A$ and the MG's state space by $s_t \in \delta$. s_t denotes the preferred course of action at time $t \in \mathbb{R}^+$. A machine learning method based on trial and error is called RL. Through the use of a reward system, an RL agent actively experiments with various control actions in its environment, observing the dynamics by tracking results. The environment in an MDP gives a vector showing its state, $s_t \in \delta$, at each time step $t \in \mathbb{R}^+$[?]. The agent (or control policy) sends a suitable action a_t in response to the perceived state s_t. Next, a scalar reward $r_{t+1} = r(s_t, a_t)$ is given to the agent. The state will develop to $s_{t+1} \in \delta$ as a result of this action's impact on the environment, which is represented by the state-transition probability $p(s_{t+1} \mid s_t, a_t)$. A correspondence, π, between the state and the action, which can be either deterministic or stochastic, serves as a representation of the policy. The following yields the entire discounted reward τ :

$$R_t = \sum_{k=0}^{\infty} \gamma^k r(s_{t+k}, a_{t+k}) \tag{5}$$

Regression

The Q-table becomes unfeasible when Deep Q-Learning is applied in scenarios where the state-action space is large or infinite. This challenge can be solved by reconstituting the Q-table using a non-linear form, like function approximation, which treats the task as a supervised learning task similar to regression. The rising ability of deep neural networks to handle complicated systems with high dimensions made them an attractive option for

estimating the action value function. This methodology's inception dates back to Mnih et al.'s 2015 debut of Deep Q-Network (DQN) [19]. Deep Q-Learning has challenges that make the Q-table unfeasible when dealing with settings where the state-action space is large or infinite. This problem can be resolved by reconstructing the Q-table in a non-linear form, like function approximation, and treating it as a supervised learning task akin to regression. Power electronics converters can use regression to find a relationship between input and output variables. Regression analysis is mostly used in power electronics converters to predict the value of the input signal to obtain the intended output [20].

The connection between the input and output variables varies depending on the type of converter. Certain relationships might only be solved by non-linear regression as the boost converter, whereas others might be solved by linear regression as the buck converter, which has been used in this paper. The solution to linear regression involves fewer steps and less processing power than non-linear regression [21]. A polynomial of degree n is represented as Equation 6:

$$y = \beta_1 x^n + \beta_2 x^{n-1} + \beta_3 x^{n-2} + \cdots + \beta_n \tag{6}$$

A linear equation is used in the statistical technique known as linear regression to represent the association between one or more autonomous variables (X) and an affiliate variable (Y). Finding the optimum line of best fit that can accurately forecast the value of Y given a value of X is its primary objective. Equation 10 is the expanded linear regression formula for several independent variables [22].

$$Y = \beta_0 + \beta_1 X_1 + \beta_2 X_2 + \beta_k X_k + \varepsilon \tag{7}$$

Although deep reinforcement learning-based controllers perform exceptionally well on high-end computers, their limited computational capacity makes them unsuitable for end devices such as microcontrollers. To efficiently utilize this strategy on microcontrollers with limited processing capacity, this work combines a regression-based optimization technique with a more straightforward Q-table-based method [21].

Suggested Approach

Regression is used in the control system described in this paper to determine the best controller policy. It is based on RL. The duty cycles of the converter and the load quantity

highly influence how well it performs, and support vector separation has all in this paper have been mapped using the RL model. The duty cycle as well, as the relationship between load impedance, is nonlinear. To supply the required PWM signal, the model makes use of a second-order exponential formula as the guideline. To enhance the guidelines system makes use of optimization based on nonlinear backwardness. Nonlinear regression techniques are employed by the RL model to improve the policy through the use of Q-table data. The PWM of the duty cycle acts as the model's action, while the output impedance of the load acts as its state. It features an immediate load impedance and a voltage-tracking loop. The output voltage at the load bus and the shunt voltage drop are used to track the load impedance. Equations 8 show how the RL model is applied to the Q table update. After deciding if the current action is better than the previous one for the given state, the procedure logs the reward for the current state-activity pair. With a single operation, the controller can provide the desired result under any condition. As such, the team does not need to consider prospective future benefits in addition to past rewards when rewarding any state-action pair.

$$SR_{\max} = \begin{cases} SnR & \text{if } 23.9 < \text{ voltage } < 24.1 \\ & \text{and SnR} = | \text{ voltage } - 24 | \\ & \text{and } SR_{\max} < \text{SnR} \\ SR_{\max} & \text{otherwise} \end{cases} \tag{8}$$

Where, it starts by obtaining the PWM and voltage readings. It will compute the highest reward $SR_{\max}$ for the current state if the voltage is between 23.9 and 24.1 . It then computes the new reward SnR as the absolute difference between the voltage and 24 . In the event that $SR_{\max}$ is less than SnR, the process will update $SR_{\max}$ to SnR before coming to an end.

To implement the proposed controller in this experiment, state-action pairing rewards are first recorded in a reward matrix. An initial policy function is defined by the controller, and it is optimized. Subsequently, the software determines whether to add a reward for a new state-action pair by analyzing data from the Q table. If this is the case, regression iterations are used by the software to improve and optimize the policy function. The policy function is used to generate the appropriate PWM signals after the load impedance has been measured. This is illustrated by Algorithm1.

Algorithm 1 Policy Update Algorithm

```
Start
Define Q matrix
Define a policy function
while true do
    Read data from Q table
    if n(S, A) > np(S, A) then
        for i ← 0 to 49 do
            Iterate for the best policy
        end for
        np(S, A) ← n(S, A)
    end if
    Read the load impedance
    Calculate PWM
    Write PWM
    Update Q table
end while
```

A randomly chosen second-order exponential function serves as the policy's initial value. The controller generates PWM data that powers the converters of the MG, which switches loads attached to its output at predetermined intervals. The policy function begins to optimize when the duty cycle, which adapts to different load scenarios, as shown in (9).

Figure 15. Reinforcement Learning Controller in the Proposed DC Microgrid

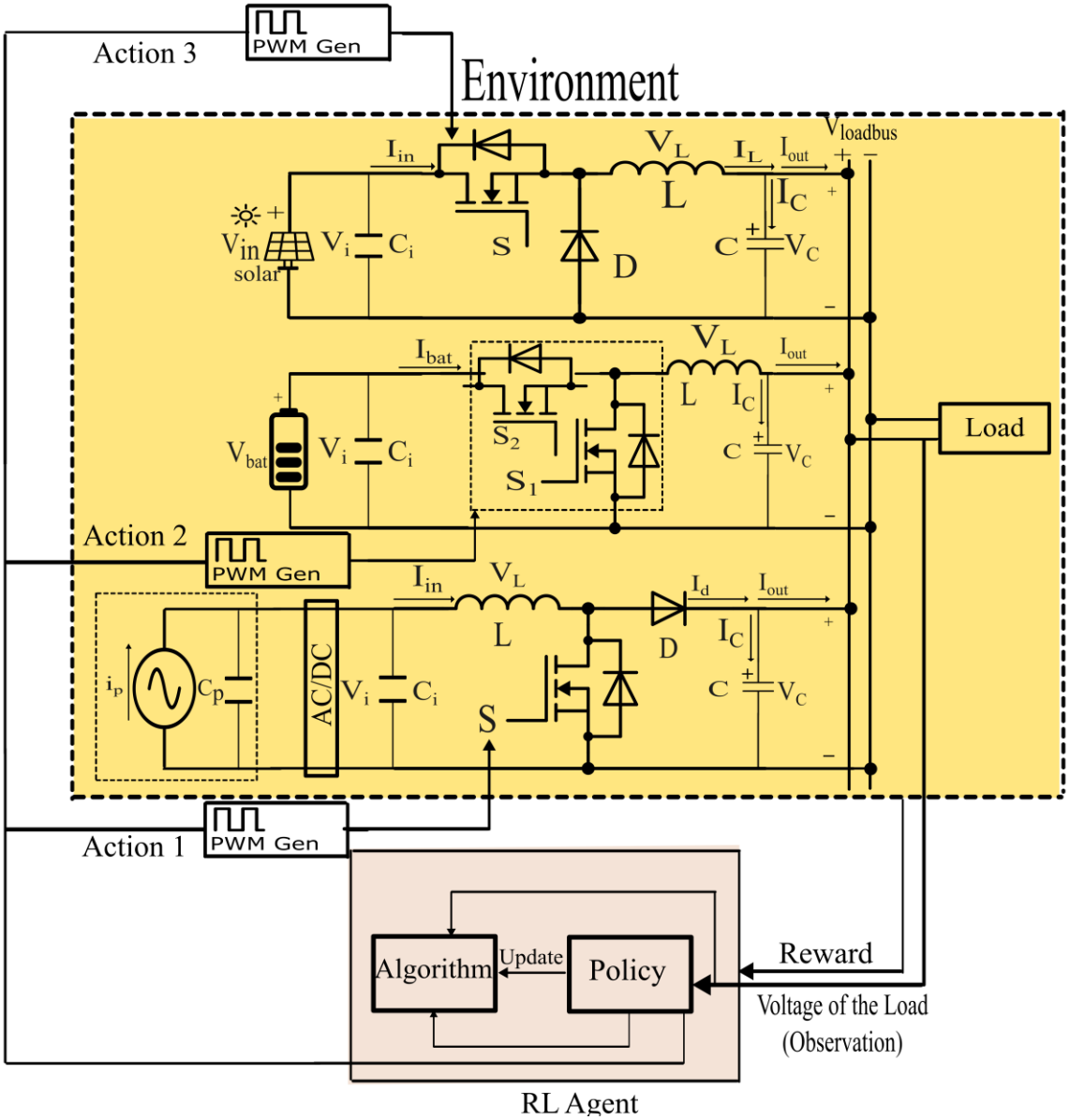

$$f(R_n) = ae^{bRn} + ce^{dR_n} \tag{9}$$

The RL agent will compute a, b, c, and d using the described policy, where the values are $a = 6.56, b = -0.54, c = 0.31$, and $d = -0.032$. These values will be applied to the transfer function for the boost converter. As the duty cycle changes to account for changing loads, the policy function for the buck converter begins to optimize, as

demonstrated in 10, but now employs a linear function as the buck converter has a linear rather than exponential behavior, as depicted in Figure 11.

$$f(R_n) = aR_n + b \tag{10}$$

Following this strategy, the RL agent computes the coefficients a and b, which have the values $a = 0.00839, b = 0.4897$. In order to compare the suggested MG controller to the PI in terms of robustness, four failure scenarios will be examined. Figure 15 shows how RL is implemented in the DCHMG.

Discussion of Results

Short Circuit Across the Load

Typically, in DCHMG systems, failures in power converters related to the AC side, including voltage source converters or short circuits in transmission and distribution lines, may result in AC side breakdowns. Conversely, DC faults can be short-circuit faults such as arc, line-to-ground (L2G), and line-to-line (L2L). When a system malfunctions, converters' operating points drastically change [23]. The DC load bus voltages will drop and vary if the controller cannot handle such situations, which will de-energize the entire system. Furthermore, there is a chance of fire dangers based on the nature and location of the fault. Thus, it is imperative that short-circuit defects be taken into account when evaluating the resilience and reliability of converters [24]. In light of the previously indicated concerns, we carried out a comparison analysis to illustrate the resilience of the suggested approach. Tests were conducted using a short-circuit fault state across the load on both the PI and the suggested technique. Figure 16 illustrates how the fault occurred at t=1 and was fixed at t=1.1. As can be shown in Table 2, the RL outperforms the PI in terms of performance, with an approximately 6% lower overshoot and a reduced undershoot of about 11%. Furthermore, the RL is considerably diminished with the peak-to-peak value. While the RL performs better overall, its steady-state error is slightly greater than that of the PI.

Figure 16. Voltage Response with Short Circuit Across Load

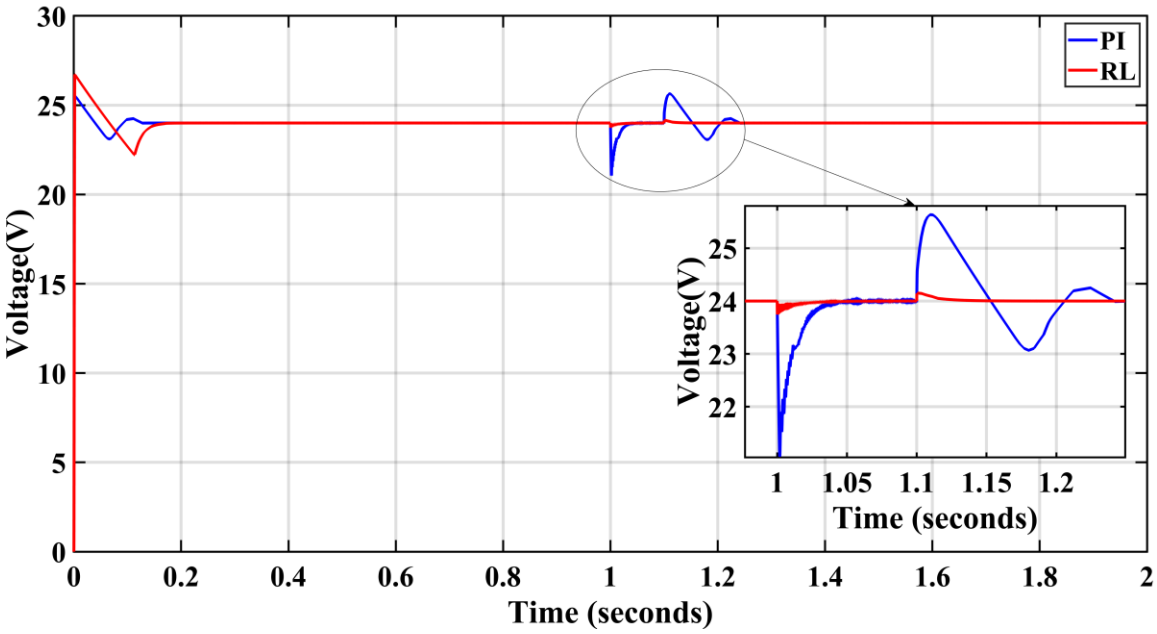

A bar chart comparing the integral of absolute error (IAE), integral of time-weighted absolute error (ITAE), and integral of squared error (ISE) is shown in Figure 17. In SC fault circumstances, the RL-based control approach works better than the PI, resulting in reduced IAE, ITAE, and ISE values. This demonstrates how well it can minimize deviations from the target amount of load voltage when compared to a PI.

Figure 17. Control Metrics Comparison for the Short Circuit

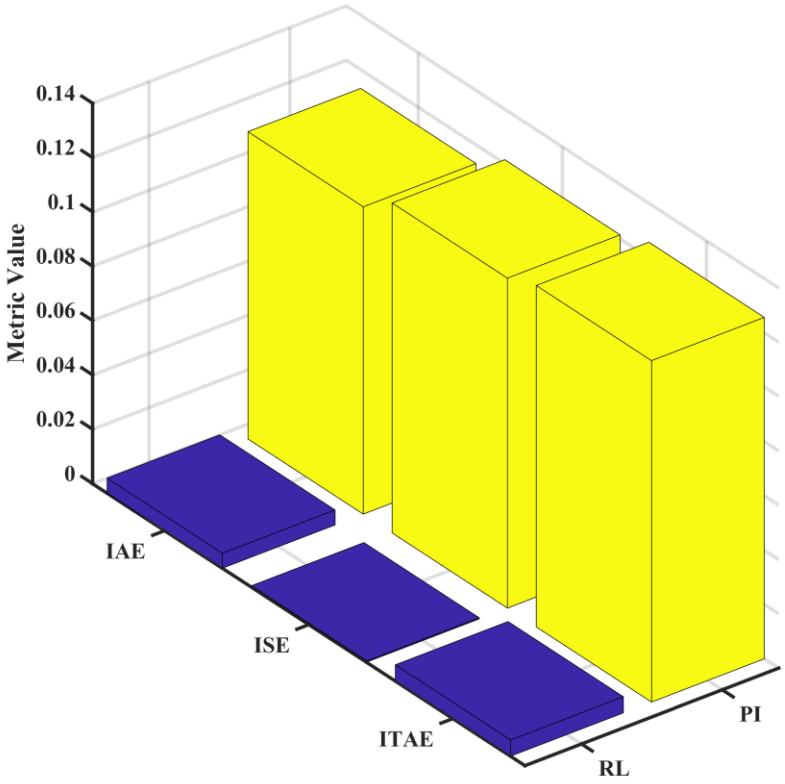

Converter Failure

The breakdown of a converter has similar negative consequences in a DCHMG but with unique subtleties. The associated loads' power supply being disrupted is the immediate result. In DCHMGs, voltage stability is especially important, and when it fails, the system as a whole may experience significant voltage variations[25]. Tests were applied on both RL and PI in the failure of one of the converters. This failure occurred at $t = 1$ and was rectified at $t = 1.1$, as seen in 18.TABLE 2 shows that the RL controller performs better in terms of both overshoot and undershoot; but, because of the harshness of the scenario, the improvements are not statistically significant. Still, the RL performs better than of PI.

Figure 18. Voltage Response with Converter Failure

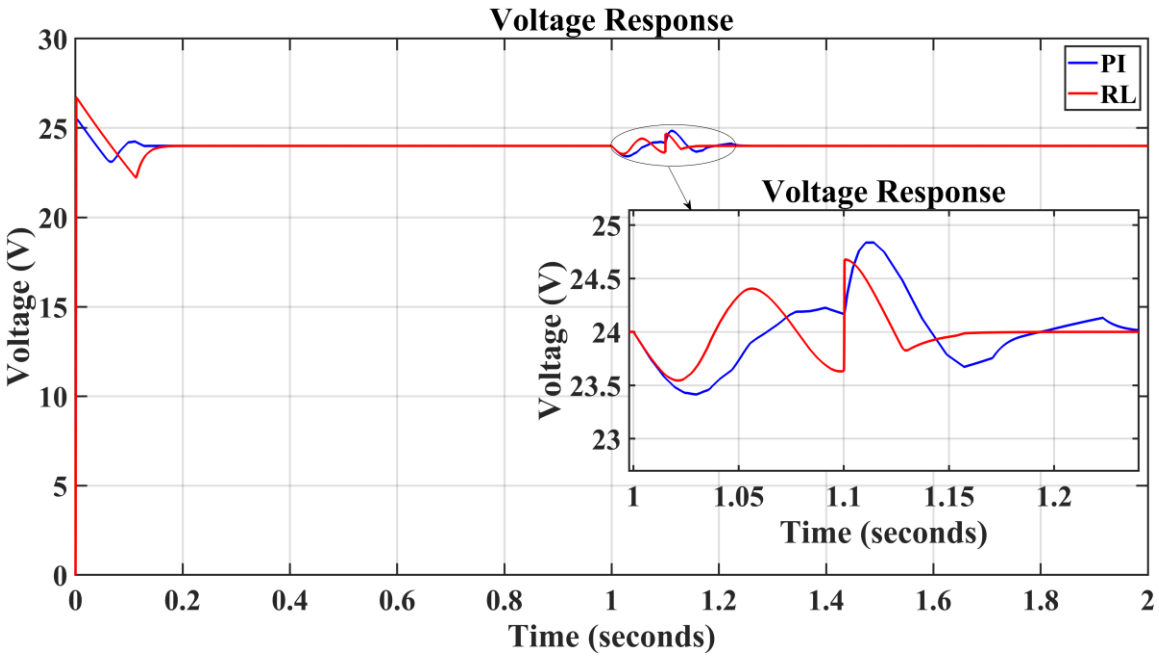

A comparison bar chart between IAE, ITAE, and ISE error measurement criteria is shown in Figure 19. With lower control metric values during converter failure, the RL outperforms the PI in terms of performance. In comparison to the PI, this highlights its capacity to keep load voltage closer to the desired level and hence minimize deviations.

Figure 19. Control Metrics Comparison for Converter Failure

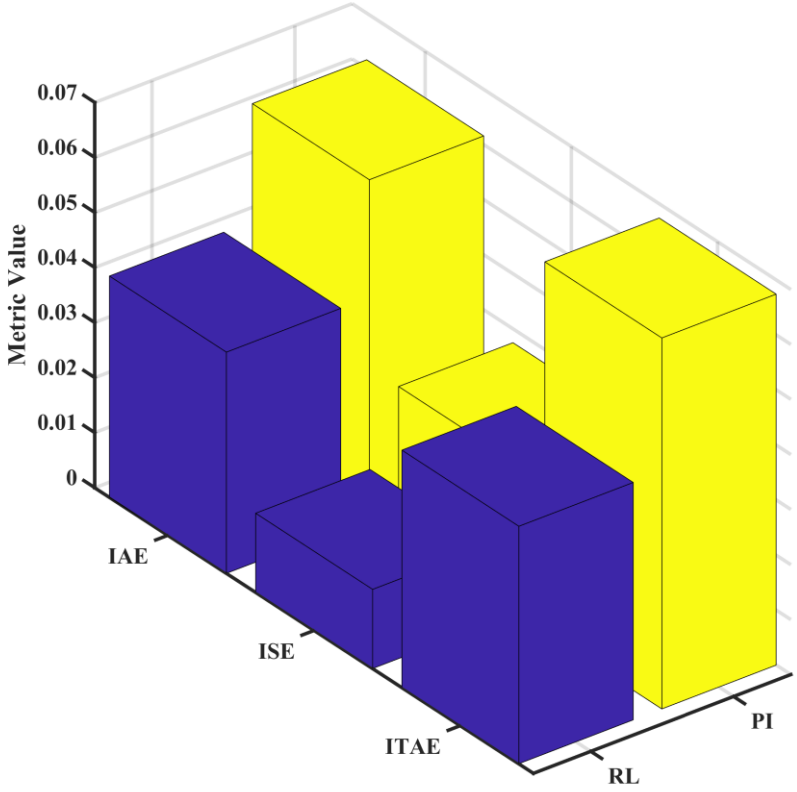

Load Variation

One of the important duties of the controllers in a DCHMG is to oversee the installation and removal of loads. During these transitions, the controller must efficiently restore and maintain voltage stability to guarantee the overall stability and reliability of the MG. To assess this situation, Figure 20 shows how a significant load was added to the system at $t = 1$. With an undershoot of over 8% and a steady-state error of approximately 3% less than the PI, the RL performs noticeably better than the PI.

Figure 20. Voltage Response with sudden changes in the load

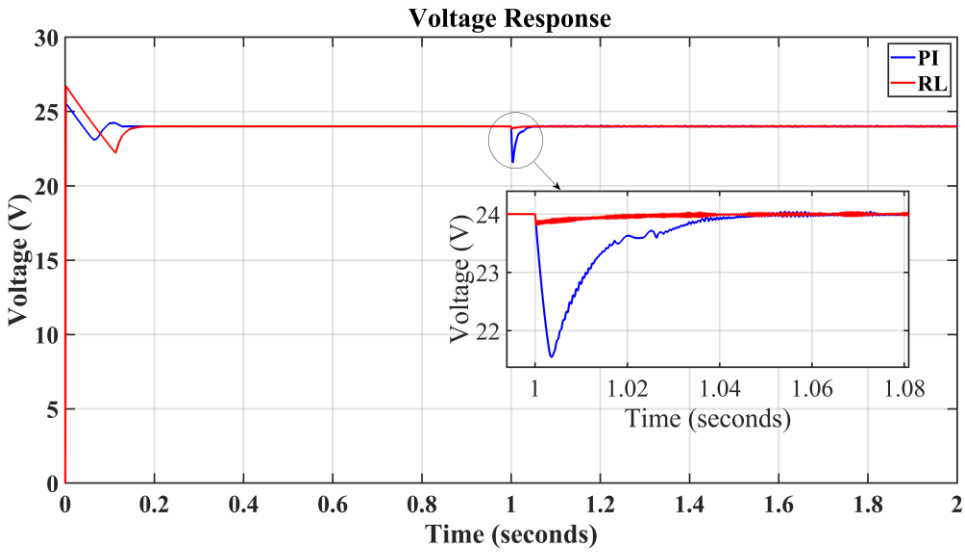

Figure 21 presents a bar chart that contrasts the error metrics of the two controllers. It demonstrates that the ISE of the RL is roughly 3% lower than that of the PI and that its IAE and ITAE are nearly 2% lower.

Figure 21. Control Metric Comparison for Load Variation

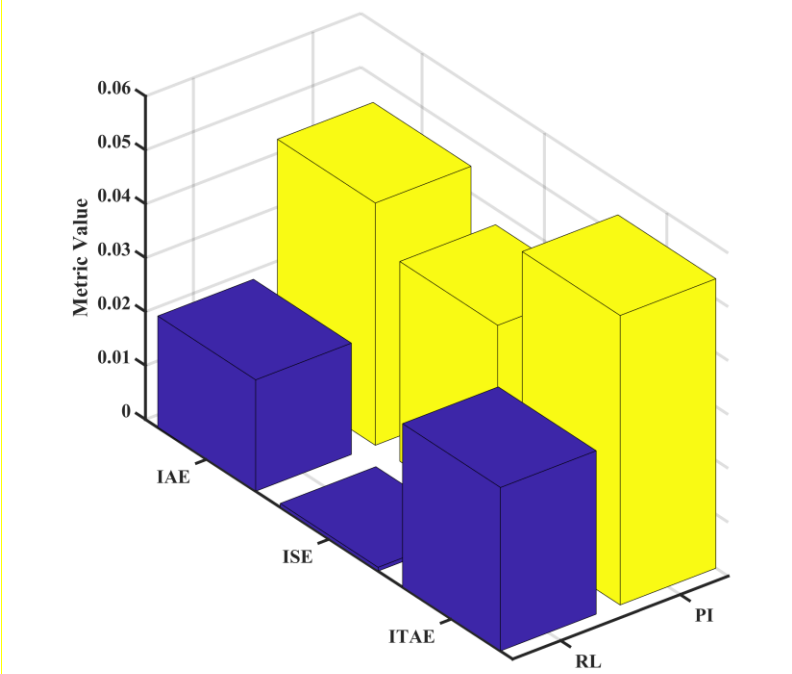

Open Circuit of the Load

When parts are detached for normal maintenance or equipment replacement, there may be a brief period of an open circuit. This may happen without the previous notice of the maintenance crew and the engineers, so the controller must be able to restore voltage to its nominal value. Any break or disconnect in the electrical channel that stops electricity from passing through the circuit and causes the linked load to lose power is known as an open circuit. To replicate this, a breaker disconnects the load at $t = 1$ and reconnects it at $t = 1.1$. The controller is responsible for restoring voltage during this scenario. The RL shows less undershoot and overshoot by almost 2% and much less peak-to-peak amount than the PI. Although the steady-state error of RL is slightly more, the overall performance of RL is better, as depicted in Figure 22.

Figure 22. Voltage Response with Open Circuit Across the Load

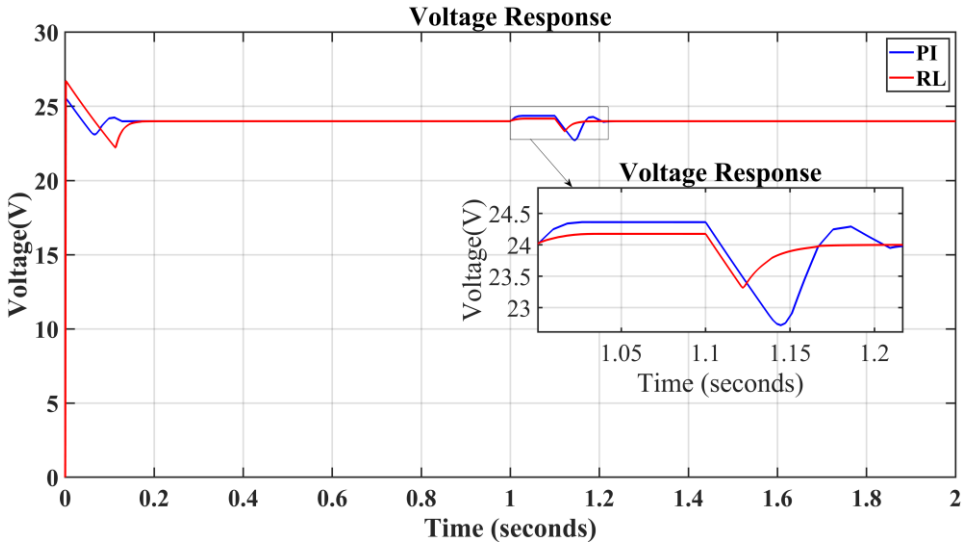

According to Figure 23, the suggested controller has IAE and ITAE control metrics that are over 2% and 4% lower, respectively, than the PI.

Figure 23. Control Metrics Comparison for Open Circuit Across the Load

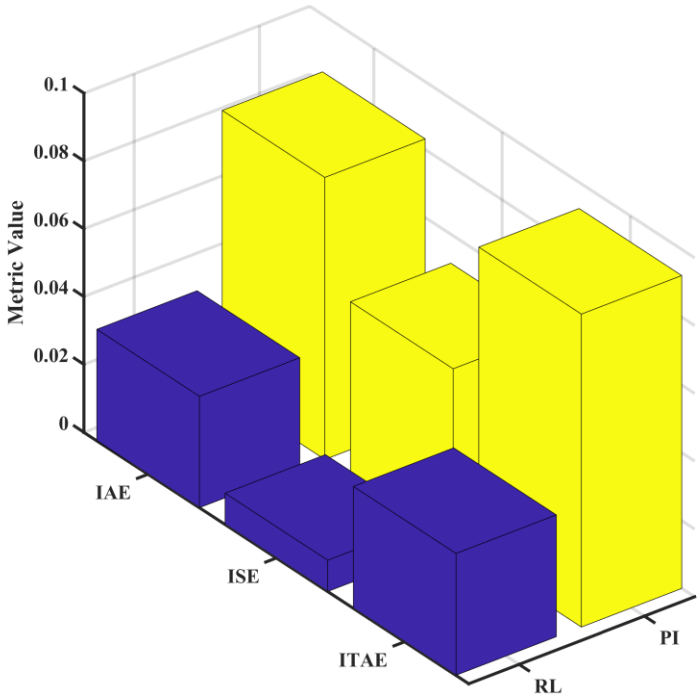

A thorough comparison of the two controllers is given in Table 2. The acronyms used in the table are: CF for Converter Failure; LV for Load Variation; OCL for Open Circuit of the Load; and SCL for Short Circuit across the Load Variation.

Table 2. Controllers Behaviors Under Various Fault Scenarios

Controller	RL	PI	RL	PI	RL	PI	RL	PI
Metrics	*Scenarios*							
	SCL (%)		OCL (%)		CF (%)		LV (%)	
Steady State Error	0.07	0.03	0.078	0.02	0.06	0	1.79	4.12
Overshoot	0.63	6.82	0.73	1.51	2.90	3.48	0.22	0.34
Undershoot	1.07	12.28	2.83	5.33	1.91	2.44	0.82	10.22
Peak-to-Peak	40.62	458.3	85.5	164.12	115.54	142.16	25.03	253.69
IAE	0.55	11.31	3.35	8.31	4.01	6.15	2.06	4.45
ISE	0.04	12.14	0.91	5.16	1.44	2.75	0.07	3.70
ITAE	0.59	12.57	3.56	9.25	4.31	6.74	3.03	5.37

Conclusions

This study introduces a resilient control scheme for a hybrid DC microgrid (DCHMG) integrating solar, battery storage, and piezoelectric harvesters. The MG serves as an energy hub to supply electricity to lighting systems in the transportation sector, such as roads. In this study, the piezoelectric harvesters were modeled using experimental data from a traffic simulator. The proposed RL method was tested under four severe and unexpected failure scenarios: a short circuit at the load side, a sudden and severe change in load, an open circuit, and converter failure. The performance of the control scheme was compared with a benchmark controller (i.e., PI control scheme). Results show the effectiveness of the proposed controller in improving the resilience of the energy hub under test.

Recommendations

In the future, it is essential to further assess the economics, reliability, and durability of piezoelectric modules to enhance their viability in practical applications.

References

1. M. H. Saeed, W. Fangzong, B. A. Kalwar, and S. Iqbal, "A review on microgrids' challenges & perspectives," *IEEE Access*, vol. 9, pp. 166502-166517, 2021.
2. W. Strielkowski, L. Civín, E. Tarkhanova, M. Tvaronavičienė, and Y. Petrenko, "Renewable energy in the sustainable development of electrical power sector: A review," *Energies*, vol. 14, p. 8240, 2021.
3. M. B. Abdelghany, A. Al-Durra, and F. Gao, "A coordinated optimal operation of a grid-connected wind-solar microgrid incorporating hybrid energy storage management systems," *IEEE Transactions on Sustainable Energy*, vol. 15, pp. 39-51, 2023.
4. M. Edla, Y. Y. Lim, D. Mikio, and R. V. Padilla, "A Single-Stage Rectifier-Less Boost Converter Circuit for Piezoelectric Energy Harvesting Systems," *IEEE Transactions on Energy Conversion*, vol. 37, pp. 505-514, 2022.
5. E. Lefeuvre, D. Audigier, C. Richard, and D. Guyomar, "Buck-Boost Converter for Sensorless Power Optimization of Piezoelectric Energy Harvester," *IEEE Transactions on Power Electronics*, vol. 22, pp. 2018-2025, 2007.
6. S. Bairagi, S. ul Islam, M. Shahadat, D. M. Mulvihill, and W. Ali, "Mechanical energy harvesting and self-powered electronic applications of textile-based piezoelectric nanogenerators: A systematic review," *Nano Energy*, vol. 111, p. 108414, 2023.
7. S. X. Long, S. Khoo, O. Chao, and M. Soong, "Finite element analysis of a dual-layer substrate sandwiched bridge piezoelectric transducer for harvesting energy from asphalt pavement," presented at the 2019 IEEE SENSORS, 2019, pp. 1-4.
8. J. Q. S. T. B. X. A. Yazdani, "Ultra-High Power Density Roadway Piezoelectric Energy Harvesting System," 2023, pp. 1-42.
9. P. Yingyong, P. Thainiramit, S. Jayasvasti, N. Thanach-Issarasak, and D. Isarakorn, "Evaluation of harvesting energy from pedestrians using piezoelectric floor tile energy harvester," *Sensors and Actuators A: Physical*, vol. 331, p. 113035, 2021.
10. N. Rezaei-Hosseinabadi, A. Amoorezaei, A. Tabesh, S. A. Khajehoddin, R. Dehghani, and K. Moez, "A Voltage-Feedback-Based Maximum Power Point Tracking Technique for Piezoelectric Energy Harvesting Interface Circuits," *IEEE Internet of Things Journal*, vol. 11, pp. 20433-20442, 2024.
11. Y. Feng, M. Liang, and Y. Li, "Adaptive Controller With Anti-Windup Compensator for Piezoelectric Micro Actuating Systems," *IEEE Transactions on Nanotechnology*, vol. 23, pp. 45-54, 2024.

12. J. Forrester, J. N. Davidson, and M. P. Foster, "Inductorless Step-Up Piezoelectric Resonator (SUPR) Converter: A Describing Function Analysis," *IEEE Transactions on Power Electronics*, vol. 38, pp. 12874-12885, 2023.

13. Z. Li et al., "Piezoelectric Energy Harvesting Interface Using Self-Bias-Flip Rectifier and Switched-PEH DC-DC for MPPT," *IEEE Journal of Solid-State Circuits*, vol. 59, pp. 2248-2259, 2024.

14. H. Mahmood, D. Michaelson, and J. Jiang, "A Power Management Strategy for PV/Battery Hybrid Systems in Islanded Microgrids," *IEEE Journal of Emerging and Selected Topics in Power Electronics*, vol. 2, pp. 870-882, 2014.

15. I. A. Galkin, R. Saltanovs, A. Bubovich, A. Blinov, and D. Peftitsis, "Considerations on Combining Unfolding Inverters with Partial Power Regulators in Battery-Grid Interface Converters," *Energies*, vol. 17, 2024.

16. M. Mahazabeen, A. J. Abianeh, S. Ebrahimi, H. Daoud, and F. Ferdowsi, "Enhancing EV charger resilience with reinforcement learning aided control," *e-Prime - Advances in Electrical Engineering, Electronics and Energy*, vol. 5, p. 100276, 2023.

17. M. Seyedi, K. Sheida, S. Siner, and F. Ferdowsi, "Enhanced Resilience in Battery Charging through Co-Simulation with Reinforcement Learning," 2024.

18. K. Sheida, M. Seyedi, and F. Ferdowsi, "Adaptive Voltage and Frequency Regulation for Secondary Control via Reinforcement Learning for Islanded Microgrids," in *Proc. 2024 IEEE Texas Power and Energy Conference (TPEC)*, 2024, pp. 1-6.

19. R. S. Sutton and A. G. Barto, *Reinforcement learning: An introduction*, MIT Press, 2018.

20. S. Zhao, F. Blaabjerg, and H. Wang, "An overview of artificial intelligence applications for power electronics," *IEEE Transactions on Power Electronics*, vol. 36, pp. 4633-4658, 2020.

21. A. Marahatta, Y. Rajbhandari, A. Shrestha, S. Phuyal, A. Thapa, and P. Korba, "Model predictive control of DC/DC boost converter with reinforcement learning," *Heliyon*, vol. 8, p. e11416, 2022.

22. Y. Saeidinia, M. Arabshahi, M. Aminirad, and M. Shafie-khah, "Enhancing DC microgrid performance through machine learning-optimized droop control," *IET Generation, Transmission & Distribution*, vol. 18, pp. 1919-1934, 2024.

23. N. Yadav and N. R. Tummuru, "Short-Circuit Fault Detection and Isolation Using Filter Capacitor Current Signature in Low-Voltage DC Microgrid Applications," *IEEE Transactions on Industrial Electronics*, vol. 69, pp. 8491-8500, 2022.

24. H. Tarzamni, F. P. Esmaeelnia, F. Tahami, M. Fotuhi-Firuzabad, P. Dehghanian, M. Lehtonen, and F. Blaabjerg, "Reliability Assessment of Conventional Isolated PWM DC-DC Converters," *IEEE Access*, vol. 9, pp. 46191-46200, 2021.

25. S. Zhou et al., "On the Resilience Analysis of DC Microgrids With Power Buffer Control," *IEEE Transactions on Circuits and Systems I: Regular Papers*, 2024, pp. 1-14.